Spontaneously exsolved free gas during major storms as a driver for pockmark formation

S. Gupta[1], C. Schmidt[1], C. Böttner[2], L. Rüpke[1], and E. H. Hartz[3,4]

[1]GEOMAR Helmholtz Center for Ocean Research, Wischhofstr. 1-3, Kiel, 24148, Germany
[2]Institute of Geosciences, Christian-Albrechts-Universität zu Kiel, Otto-Hahn-Platz 1, Kiel, 24118, Germany
[3]AkerBP, Lysaker, Norway
[4]Centre for Earth Evolution and Dynamics (CEED), University of Oslo, Norway

Key Points:

- Storm-induced pressure changes can lead to spontaneous appearance of free gas phase near the seafloor.
- This process is driven by pressure-sensitive phase instabilities.
- This mechanism could help explain elusive gas sources in recently observed pockmarks in the North Sea.

Corresponding author: Shubhangi Gupta, sgupta@gmail.com

Abstract

Abrupt fluid emissions from shallow marine sediments pose a threat to seafloor installations like wind farms and offshore cables. Quantifying such fluid emissions and linking pockmarks, the seafloor manifestations of fluid escape, to flow in the sub-seafloor remains notoriously difficult due to an incomplete understanding of the underlying physical processes. Here, using a compositional multi-phase flow model, we test plausible gas sources for pockmarks in the south-eastern North Sea, which recent observations suggest have formed in response to major storms. We find that the presence of free gas in the subsurface effectively damps storm wave-induced pressure changes due to its high compressibility, so that the mobilization of pre-existing gas pockets is unlikely. Rather, our results point to spontaneous appearance of a free gas phase via storm-induced gas exsolution from pore fluids. This mechanism is primarily driven by the pressure-sensitivity of gas solubility. We show that in highly permeable sediments containing gas-rich pore fluids, wave-induced pressure changes result in the appearance of a persistent gas phase. This suggests that seafloor fluid escape structures are not always proxies for overpressured shallow gas and that periodic seafloor pressure changes can induce persistent free gas phase to spontaneously appear.

Plain Language Summary

Thousands of pockmarks were reported in North Sea, presumably formed in response to wave motions during major storms. It has been hypothesized that these pockmarks formed as pre-existing shallow free-gas pockets were mobilized by pressure changes of the waves. However, mechanisms that could have mobilized free-gas are not yet constrained. Moreover, large scale free-gas accumulations have not been reported in this region, and therefore, commonly invoked mechanisms like tensile failure and breaching of capillary seals are hard to justify as they rely on the presence of pre-existing gas pockets. Here, through modelling studies, we tackle the question of the source of the observed free-gas. Our study consists of two parts: First, assuming that some hitherto unknown shallow free-gas pocket is indeed present, we test whether storm-induced pressure changes could breach capillary seals. We find that free-gas damps pressure changes due to its high compressibility, making the mobilization of pre-existing gas unlikely. In the second part, we propose an alternative mechanism where free-gas spontaneously appears due to exsolution from pore-fluids. We test the feasibility of this mechanism and show how periodic pressure changes can lead to a persistent gas phase, that could explain the elusive gas source linked to these pockmarks.

1 Introduction

Fluid and gas flow in shallow marine sediment play a key role in the Earth System by modulating the chemical exchange between the seafloor and the water column (Boetius et al., 2000; Whiticar, 2002; Berndt, 2005; A. G. Judd, 2003; A. Judd & Hovland, 2007; Talukder, 2012). Abrupt fluid emissions are also a geohazard to marine infrastructures (Sills & Wheeler, 1992) such as wind parks (Lundsten et al., 2019) and offshore cables, which host over 95% of intercontinental data traffic (Carter, 2010). Pockmarks, semi-circular depressions of the seafloor, can be the manifestations of fluid release (Hovland & Sommerville, 1985; Dando et al., 1991; A. Judd et al., 1994; Hovland et al., 2002). They have diameters ranging from a few meters up to over a kilometer, and depths from tens of centimeters to several meters (A. Judd & Hovland, 2007). Since their discovery in the 1970's (King & McLean, 1970), pockmarks have been in the focus of scientific investigations as they may indicate the release of greenhouse gases such as methane from marine sediments (Dando et al., 1991; Boetius et al., 2000; Hovland et al., 2002; Berndt, 2005). The increasing availability of high-resolution bathymetric data has revealed their

worldwide abundance and importance (A. Judd & Hovland, 2007; Feldens et al., 2016; Krämer et al., 2017; Böttner et al., 2019; Hoffmann et al., 2020).

The formation of pockmarks has been primarily attributed to the release of hydrocarbons from overpressured gas reservoirs beneath the seafloor (Böttner et al., 2019; Feldens et al., 2016; A. Judd & Hovland, 2007). In this scenario, a pockmark forms when the gas overpressure exceeds the tensile failure envelope leading to gas escape and subsequent sediment erosion at the seafloor. Fluid escape itself can take place as continuous seepage flow (Böttner et al., 2019; Dumke et al., 2014), episodic/pulsed flow (Hoffmann et al., 2020; von Deimling et al., 2011), single blow-out events (Løseth et al., 2011; Andreassen et al., 2017) or a combination of those, e.g. where blow-out events are followed by continuous seepage (Leifer & Judd, 2015; von Deimling et al., 2015). The type of flow can vary depending on the subsurface pressure, stress states, and lithological conditions. Therefore, the activity of a fluid-escape structure may exhibit temporal variability, which may be cyclic over both short time scales such as tidal cycles (Boles et al., 2001; Rollet et al., 2006; Römer et al., 2016) or longer-term sea level changes (Plaza-Faverola et al., 2011; Riboulot et al., 2014).

There is emerging evidence that pockmarks can also form spontaneously forced by major storms associated with significant wave heights. Krämer et al. have presented hydroacoustic data from the south-eastern North Sea that shows abundant and very densely spaced pockmarks (Fig.1 a,b. These pockmarks were not reported previously from the area and appear to have formed over three months during storm events in the fall of 2015 (Krämer et al., 2017). These pockmarks vanished during calmer weather conditions, possibly through residual sediment transport in response to tidal forcing. In 2018, expedition AL512 found no remaining traces of the pockmark field (Karstens et al., 2018).

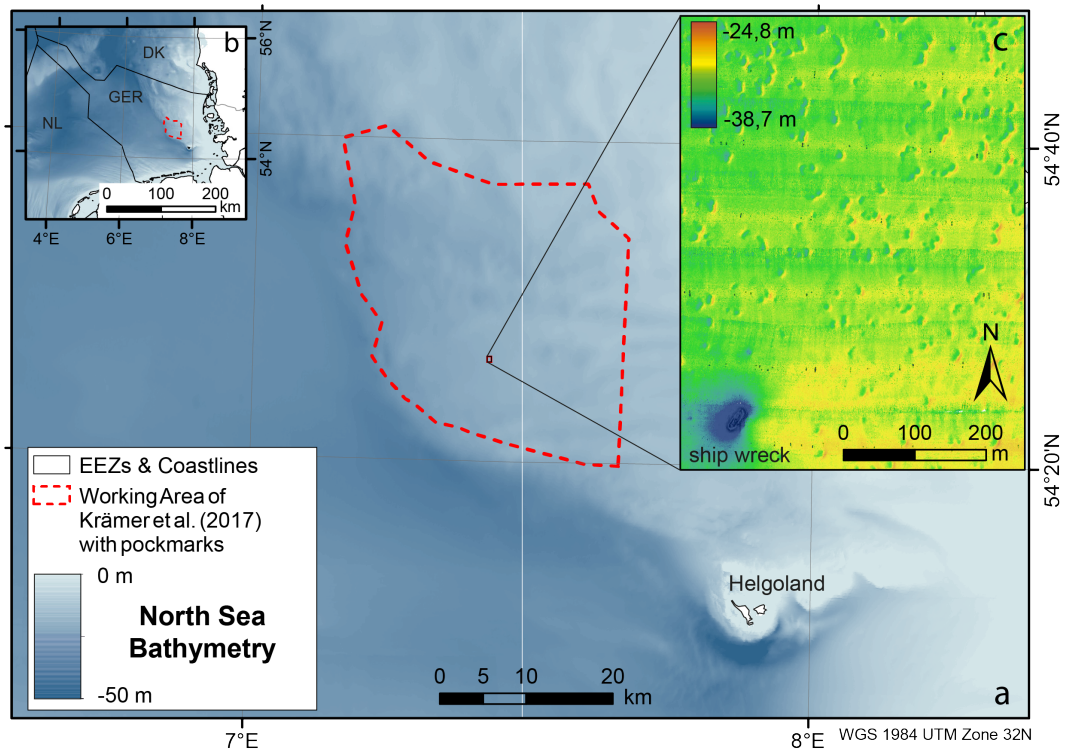

Figure 1: (a) Bathymetric map of working area in the North Sea. (b) Overview map showing working area in the southeastern North Sea. (c) Detailed bathymetric map showing Pockmarks on the seafloor of the Helgoland Reef (data from Krämer 2017).

Linking pockmarks to hydro-mechanical processes in the sub-seafloor remains notoriously difficult. It requires constraining how gas is mobilized towards the seafloor and which sedimentary processes 'make' the morphological pockmark in response to gas and fluid venting. Here we focus on the first problem. One plausible formation scenario of the aforementioned pockmarks in the North Sea is that storm wave-induced pressure changes mobilized shallow gas accumulations within the sediments (Krämer et al., 2017) by either inducing tensile failure or helping the gas to overcome its capillary seal. A direct implication of this is that these wave-induced pockmarks may be proxies for shallow gas pockets, which has major ramifications for offshore drilling and planning of seafloor installations.

Large scale shallow gas accumulations have, however, not been reported from this area. Furthermore, how fluids can overcome capillary barrier (or induce tensile failure) by short-term pressure changes remains enigmatic. This suggests that there may be an alternative mechanism that does not rely on pre-existing gas accumulations. A careful analysis of a comprehensive compositional multiphasic subsurface model for gas transport has lead us to consider the possibility that the dominant gas source for wave-induced pockmark formation could be related to pressure sensitive gas phase instabilities. This mechanism relies on local gas solubility being proportional to pore-pressure. Therefore, changes in pore-pressure will change the local gas solubility, and under the right conditions, the gas solubility may become low enough to trigger a localized spontaneous exsolution of the dissolved gases, resulting in a free gas phase that is highly unstable under the rapidly oscillating pore-pressure states. The presence of highly compressible gas is known to effectively damp pressure variations, which raises the intriguing possibility that wave-induced gas exsolution and dissolution may by asymmetric, leading to the appearance of a persistent gas phase that may rise to make a pockmark.

In this manuscript, we first test the feasibility of the 'conventional' scenario that wave-induced pressure changes can mobilize a pre-existing gas pocket. In a second step, we explore the alternative mechanism of spontaneous appearance of free gas phase due to pressure sensitive phase instabilities under high-frequency pressure changes, i.e., storm forcings.

Testing the hypotheses

Seafloor observations

Fig. 1 (a,b) shows the study area north of Helgoland in the south-eastern North Sea, the so-called Helgoland Reef area. Here, a series of storms in the fall 2015 resulted in the emergence of a pockmark field (Krämer et al., 2017). The pockmarks are described as elliptical depressions of 10 to 20 m in horizontal extent with depth of $\sim$ 20 cm (Fig.1 c). Bathymetric maps show a large spatial heterogeneity in pockmark density: Some areas have up to $\sim$ 1200 pockmarks per km^2, while directly adjacent areas show almost no pockmarks (Krämer et al., 2017). The average water depth in the area is about 25 to 40 meters and sediments mainly consist of fine- to medium-grained sands. The amount of finer-grained sediments increases in the paleo-river beds of Eider and Elbe. The area is mostly flat and the sea floor is affected by tidal currents forming wave ripples. The storm season in 2015, during which the pockmarks appeared, had a series of large storms in November. These storms were found to have had significant wave heights exceeding 7 m with periods from 8 s to 12 s and lengths between 96 m and 177 m. Such wave heights may have perturbed the effective stress state of the top 3.5 to 7 m, yet no direct seismic or hydro-acoustic evidence exists for shallow gas pockets within these surface sediments (Krämer et al., 2017). Nevertheless, the area is known to host sediments with significant organic carbon contents, so any gas present is likely of microbial origin. Methane concentrations in the pockmark field were $\sim 30.4 \mu M$, almost one order of magnitude higher compared to areas with no pockmarks (Krämer et al., 2017).

Mathematical and computational model

We use a novel multi-physics simulator (Gupta et al., 2020), based on a compositional multiphase subsurface transport model framework, to test the feasibility of two different physical mechanisms of wave-induced gas mobilization that could lead to pockmark formation: 1) Mobilization of a pre-existing free gas pocket, and 2) formation of a persistent free gas phase due to pressure sensitive phase instabilities. The model considers a coupled two-phase two-component fluid system. Flow in the subsurface is assumed to follow Darcy's law, and feedbacks between the effective compressibility of the multi-phase system and the pressure state are fully resolved. The model also considers the capillary pressure effects at the gas-water phase interfaces, parameterized using a standard Brooks-Corey model. It is important to note, that unlike the long range gas migration in marine sediments, where the advective Darcy flow is typically the dominant driver of gas flow, here, in the presence of rapid and short range pressure changes, the diffusive capillary flow (see explanation following eqn.A4) and the diffusive Fickian transport appear to be equally, if not more, important. Gas can be dissolved in the pore fluids or, if concentrations exceed the solubility limit, form a free gas phase. The gas-water phase changes are modelled on the assumption of vapour-liquid-equilibrium (VLE). The resulting variational inequalities are imposed as a set of nonlinear complementary constraints, which provide a consistent transition between single and two phase models (see eqns.A7-A11). The consistent treatment of phase transitions is, infact, one of the most powerful features of this model, without which the phase instabilities cannot be reliably simulated. In this study, we consider methane as the gas phase and use an appropriate equation-of-state (Kossel et al., 2013). Note, that also other gases such as nitrogen and carbon dioxide could contribute but are not further considered here. Thermal effects and salinity effects are also ignored for simplicity. The model equations and the numerical solution scheme are summarized in Appendix A for reference.

Pressure sensitive gas phase instability

The gas solubility typically depends on pressure and temperature (Kossel et al., 2013). As the North sea water masses are generally well mixed during the stormy winter season, major changes in bottom water temperatures are unlikely during individual storm events. In addition, any seafloor temperature perturbation would only propagate approximately 20cm into the sediments throughout a 12h storm event, depending on diffusivity, which is typically in the order of $10^{-6}\ m^2/s$. On the other hand, pressure changes propagate to much larger sediment depths (Yang et al., 2015). Therefore, in this modelling study we only focus on the pressure dependence of solubility and ignore the thermal feedbacks. At higher pressure, more gas can dissolve, and vice versa. Consequently, the gas-water phase states are strongly coupled and highly sensitive to changes in pressure. In any infinitesimal volume, a sufficiently large positive perturbation of local pressure can lead to dissolution of the available free gas within this volume due to increased solubility. In the extreme case, this can lead to disappearance of the free gas phase locally (meaning, that the system goes from two-phase to single-phase state). Conversely, a sufficiently large negative perturbation of local pressure can lead to the exsolution of dissolved gas due to reduced solubility. In the case of a single-phase system, this will lead to spontaneous[1] appearance of free gas locally (meaning, the system goes from single-phase to two-phase state). This local, spontaneous, and hysteretic appearance and disappearance of free gas due to changes in pressure is referred as pressure sensitive gas phase instability. Furthermore, it is well known from multi-phase transport models (Helmig,

[1] Gas dissolution-exsolution are spontaneous processes governed by the second law of thermodynamics (Sherwood & Dalby, 2018). The notion of 'spontaneity' is closely related to change in Gibbs free energy (ΔG); A process occurs spontaneously if $\Delta G < 0$, and proceeds until equilibrium is achieved (i.e., $\Delta G = 0$).

1997) that with increasing free gas, the effective pore fluid compressibility also increases, which damps the propagation of seafloor pressure changes into the sub-seafloor. This feedback has an interesting consequence in the form of an asymmetric pore pressure evolution which may lead to the appearance of a 'persistent' free gas phase in response to periodic seafloor pressure changes.

Model setup for numerical studies

In order to test the guiding hypotheses, we formulate an idealized $1D$ setting, as shown in Fig.2, where a perfect sinusoidal storm forcing with an amplitude A and time-period T is imposed on the average sea water column of height H. The computational domain starts from the seafloor at $z = 0$ and extends up-to a depth of $z = z_{domain}$. Note that all numerical results in this manuscript are plotted along the 'depth' below the seafloor. In all runs the storm parameters were set as: Amplitude $A = 10$m and time-period $T = 12$sec. The effects of the storm appear as instantaneous pressure changes on the sea floor. Other relevant parameters were set as: Sediment and barrier porosity $\phi = 50\%$, sediment entry pressure $P_0|_{\Omega_0} = 5$ kPa, and barrier entry pressure $P_0|_{\Omega_{barrier}} = 30$ kPa.

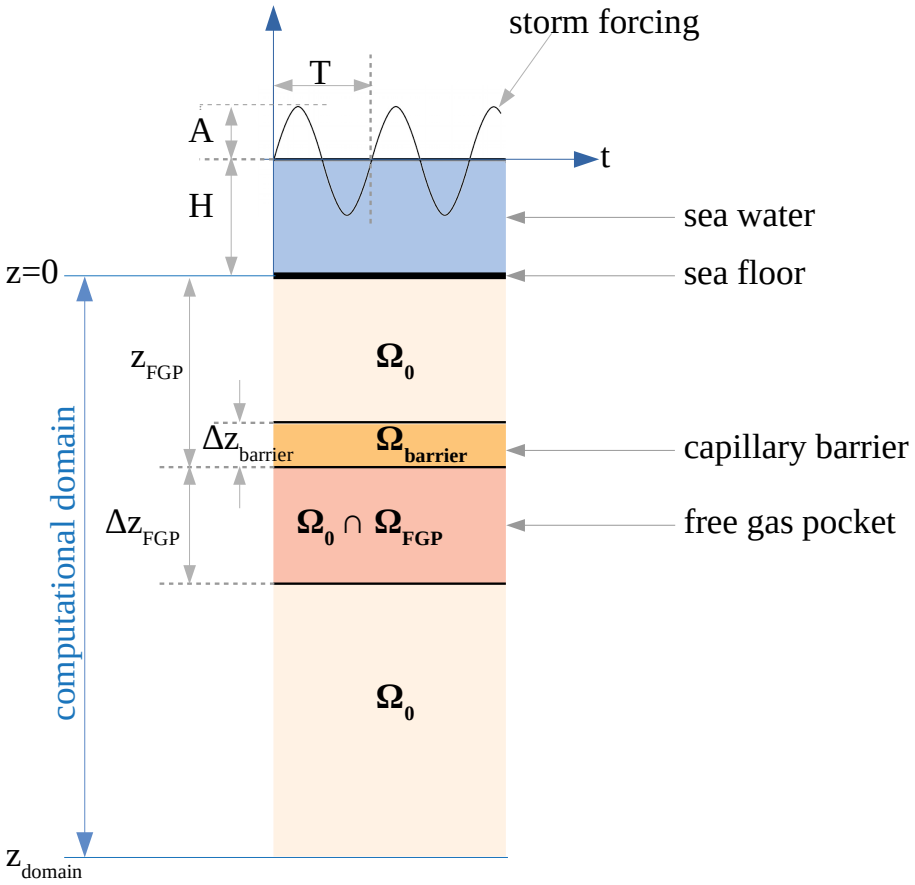

Figure 2: Conceptual model.

In model runs with a pre-existing free gas pocket (FGP), identified as Ω_{FGP} in Fig.1(d), we assume that the FGP is located at a certain depth z_{FGP} below the sea floor, and has a thickness of Δz_{FGP} and gas saturation of $S_{g,FGP}$. The FGP can only persist at this shallow depth before the storm if there exists some kind of a capillary barrier inhibiting the rapid upward migration of the free gas. This barrier can, in principle, be quite thin, but should be free of any fractures or other preferential flow paths. The most important property of this barrier is its high entry pressure, irrespective of its permeability and porosity. We consider an ideal barrier of thickness of $\Delta z_{barrier}$ ($\ll \Delta z_{FGP}$), identified as $\Omega_{barrier}$. For simplicity, the background sediment Ω_0 is assumed to be completely homogeneous and isotropic, and the effects of compaction on the porosity are ignored. Furthermore, the hydraulic properties of the background sediment and the barrier are assumed to be identical except for the entry pressure. It is clear that the likelihood of gas mobilization depends inversely on the height of the capillary barrier. For arbitrarily high capillary barriers, no practical storm forcing will be able to mobilize any volume of free gas. On the contrary, for arbitrarily low barriers, the persistence of a stable FGP can not be guaranteed. In our setting, the capillary barrier is just high enough to seal up to 80% gas saturation in the absence of any storm forcing, which gives a tenable lower bound. In this sense, we treat the capillary barrier as only an 'indirect' control. If a given storm can mobilize gas out of the FGP for such a barrier with some realistic combination of the control parameters, then we can regard pre-existing free gas pockets as a plausible gas source for the formation of pockmarks which have been linked with storm-events, especially in shallow waters. In these set of runs, we explore how water depth, permeability, and geometry as well as saturations within the FGP affect the numerical solution, and identify whether and under what conditions a storm can mobilize free gas past the capillary barrier.

In a second set of runs, we investigate the possible spontaneous appearance of a free gas phase due to the pressure sensitivity of gas solubility and the resulting phase instabilities due to the rapid storm-induced pressure changes. In addition to water depth and permeability, we also systematically vary the dissolved gas fraction and explore under which conditions a 'persistent' free gas phase forms.

In all scenarios we considered a computational domain of depth $z_{domain} = 25$m discretized into 250 finite volume cells, and chose a fixed time step size of 2 seconds for the numerical simulation of each scenario. The total duration of the storm was chosen as 10 hours.

Results

Reference model

The pressure solution for a reference sediment column subjected to the synthetic storm is shown in Fig.3. In the absence of a free gas phase, pressure oscillates around the hydrostatic value throughout the storm. It is noteworthy that the depth up to which the effect of the storm propagates depends strongly on the permeability (K) of the sediment. For $K = 10^{-14}m^2$, the depth of propagation is barely around $1m$ but increases for increasing K, and for $K = 10^{-10}m^2$ the storm propagates through the whole domain (and deeper). Note that the so-called skin-depth, the depth to which a periodic pressure oscillation propagates, is independent of water depth, yet does depend on frequency. However, we have not further investigated differing storm parameters. The grey lines in Fig.3 outline potential pressure variations in the subsurface; the actual pressure variations are strongly affected by the multi-phase phenomena that occur between the aqueous and the gaseous phase, as we will show below.

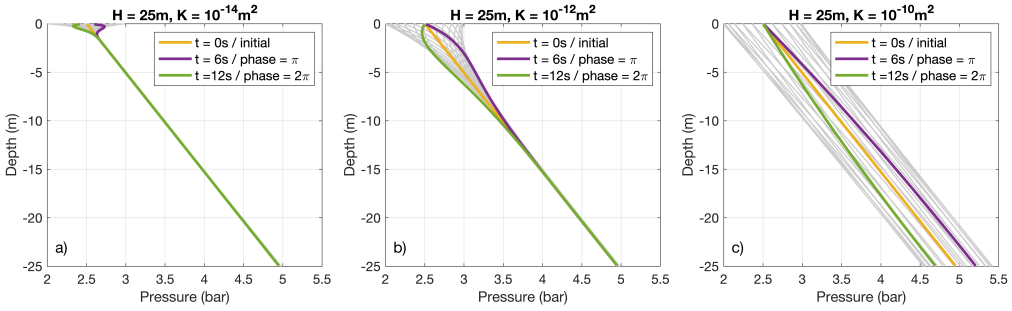

Figure 3: Range of pressure changes due to the imposed storm forcing (A=10m, T=12s) in the absence of any free gas in the domain for the 25m water depth case. The skin-depth to which the pressure perturbation propagates increases with permeability. Colored curves correspond to the initial situation (t=0s) and the zero crossings following a wave crest (t=6s) and a wave trough (t=12s); grey curves illustrates the different states over a 2π cycle.

Mobilization of pre-existing gas

In order to assess the likelihood and possible controlling mechanisms of gas mobilization from shallow accumulations during a storm, we have explored a wide parameter range. Each combination of the following control parameters was simulated: $H\,[m] = \{25, 40, 60\}$, $K\,[m^2] = \{10^{-10}, 10^{-12}, 10^{-14}\}$, $z_{FGP}\,[m] = \{2, 5, 10\}$, and $S_{g,FGP}\,[\%] = \{10, 30, 50\}$; leading to a total of 81 scenarios.

Fig.4 illustrates the system behavior in the pre-existing FGP case. The free gas phase in the FGP damps the pore pressure change due to its very high compressibility, as evidenced by the virtual absence of time-dependent pressure variations beneath the FGP (e.g., see P_g profile in Fig.4a,d). So, at the FGP-barrier interface, the pore pressure in the barrier remains greater than or equal to the pore pressure in the FGP. Note that the pressure jump at the top and bottom boundaries of the free gas zone result from the capillary pressure offset. The scenarios with low $K = 10^{-14}m^2$ (not shown) are most unremarkable because the effect of the storm forcing does not propagate up to the depth of the FGP. The barrier remains undisturbed and no free gas is mobilized.

For scenarios with moderate $K = 10^{-12}m^2$, the storm propagates up to the depth of the capillary barrier for all z_{FGP} and H under consideration, but the pressure change is not large enough to break the barrier (Fig.4a-c). All that is happening is that some dissolved methane appears within the capillary seal (Fig.4b) and that the free gas progressively accumulates beneath the capillary seal (Fig.4c) - without ever overcoming it.

All scenarios with high $K = 10^{-10}m^2$ lead to free gas phase above the seal, including cases with very low initial gas saturation of $S_{g,FGP} = 10\%$ (Fig.4f). However, this free gas does not migrate all the way to the sea-floor, even for very high initial gas saturation of $S_{g,FGP} = 50\%$ (Fig.4g-i). Within the explored parameter space, only runs with moderate ($K = 10^{-12}m^2$) to high ($K = 10^{-10}m^2$) and very shallow gas pockets ($< 2m$ depth) result in free gas close to the seafloor (not shown).

In all simulations, the gas pressure in the capillary barrier remains higher than the pressure in the FGP (meaning, that the barrier is never breached), yet some free gas escapes past the barrier. To explain this, we focus on the first few minutes of the storm. For each storm wave, the growing wave height increases pore pressure (with a phase shift and amplitude that depends on permeability and depth; see also Fig.3), which increases gas solubility (due to its pressure dependence; see Fig.4b,e) and results in the dissolu-

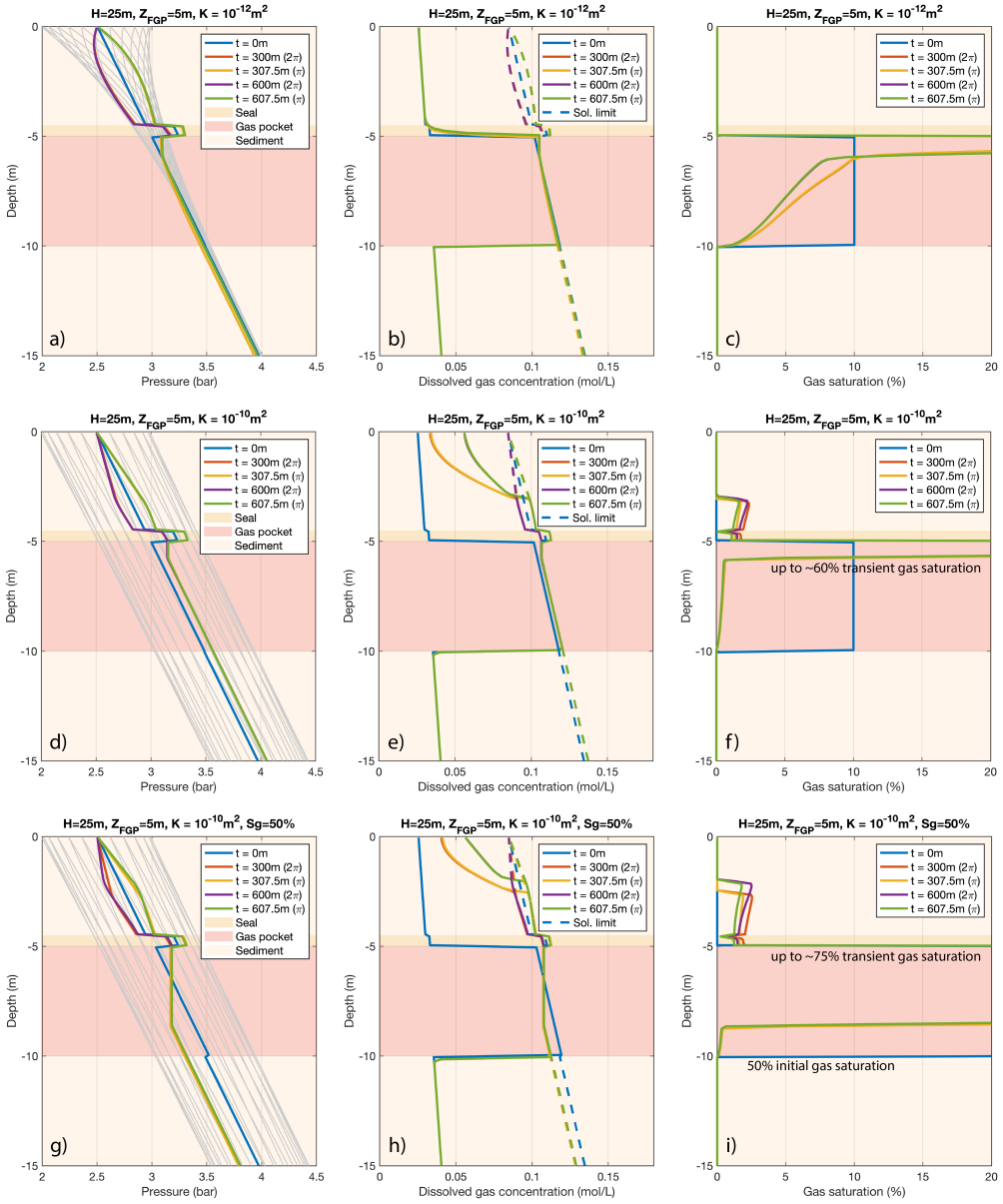

Figure 4: Gas pressure (P_g), saturation (S_g), and concentration in aq. phase (χ_g) for selected scenarios with a pre-existing FGP. For a moderate permeability ($K = 10^{-12}m^2$), waves do affect the free gas pocket but no gas is mobilized (a-c). Free gas is mobilized past the capillary barrier for high permeability ($K = 10^{-10}m^2$) but does not reach the seafloor (d-f), even for very high initial gas saturations(g-i).

tion of free gas into the aqueous phase. During the waning phase of a wave, the decreasing pressure has the opposite effect: Solubility decreases and free gas forms. This results in a pressure state that drives water with high dissolved gas concentrations out of the free gas pocket. The large jump in gas pressure across the sealing structure then causes free gas to appear above the gas pocket, again as a result of decreased solubility at lower pressure. Because gas concentrations in pore fluids within the FGP are always at the solubility limit (due to VLE), the described mechanism is asymmetric and can be thought of as a one-way valve that episodically leaks gas from the gas pocket through the seal into the sediments above. This mechanism of gas mobilization past the capillary barrier is principally driven by the pressure sensitive gas phase instability, and not the lowering of the capillary barrier. The appearance of a free gas phase above the seal also has a secondary effect: It provides a feedback to the pressure response in the next storm wave due to its high compressibility. With each successive storm wave, the pressure response dampens and less free gas appears, which can asymptotically lead to a stationary free gas phase, as observed in our scenarios with high $K = 10^{-10}m^2$.

From these observations, we can infer that it is, in general, possible for a storm to mobilize gas from a buried FGP through the mechanism of pressure sensitive gas phase instability.

Spontaneous appearance of free gas

The above simulations have shown that the pressure dependence of gas solubility is the dominant trigger for the mobilization of free gas past a capillary barrier. However, the presence of free gas above the barrier changes the subsequent pore-pressure evolution and ultimately restricts the upward migration of the mobilized free gas. These observations lead us to consider the possibility that a pre-existing buried FGP may not be the primary gas source for the emergence of storm-induced pockmarks. Instead, a free gas phase could have appeared spontaneously out of the dissolved gases during a storm due to pressure sensitive gas phase instability.

The spontaneous appearance of free gas depends on the sediment permeability, the initial amount of dissolved gas, and the pressure sensitivity of gas solubility (i.e., the slope of solubility vs. pressure curve). Permeability controls the pressure response and the advective fluxes, while the pressure sensitivity of gas solubility determines to what extent the pressure changes can suppress and enhance the gas solubility. If the pressure sensitivity of gas solubility is high, then free gas appears for lower amounts of initial dissolved gas, and vice versa. The functional dependence of gas solubility on pressure also means that the pressure sensitivity of gas solubility may be different for different hydrostatic pressure ranges. The presence of a buried FGP may 'aid' the process of pockmarks formation to some extent by acting as an additional gas reservoir, but it is neither the primary gas source nor a pre-requisite for storm-induced pockmark formation in shallow waters.

To demonstrate this mechanism, we refer back to the idealized 1D setting. We consider the same storm forcing (with parameters $A = 10$m and $T = 12$sec) and same background sediment Ω_0, but we remove the gas pocket Ω_{FGP} and the capillary barrier $\Omega_{barrier}$. An additional controlling parameter here is dissolved gas fraction $n\,[\%]$. In total, we simulated 18 scenarios for this setting choosing all combinations of the control parameters, while keeping the domain size, its discretization, and storm parameters the same as above.

For scenarios with low $n \leq 60\%$, the pressure changes affect gas solubility $\left(\chi^G_{w,eqb}\right)$ but the dissolved gas concentration remains well below the gas solubility, even for high K scenarios (not shown). In contrast, for scenarios with very high dissolved methane fraction (e.g., $n = 90\%$), the pressure changes (e.g., Fig.5a,d) suppress gas solubility below the dissolved gas concentration (e.g., Fig.5b,e) and lead to gas exsolution near the

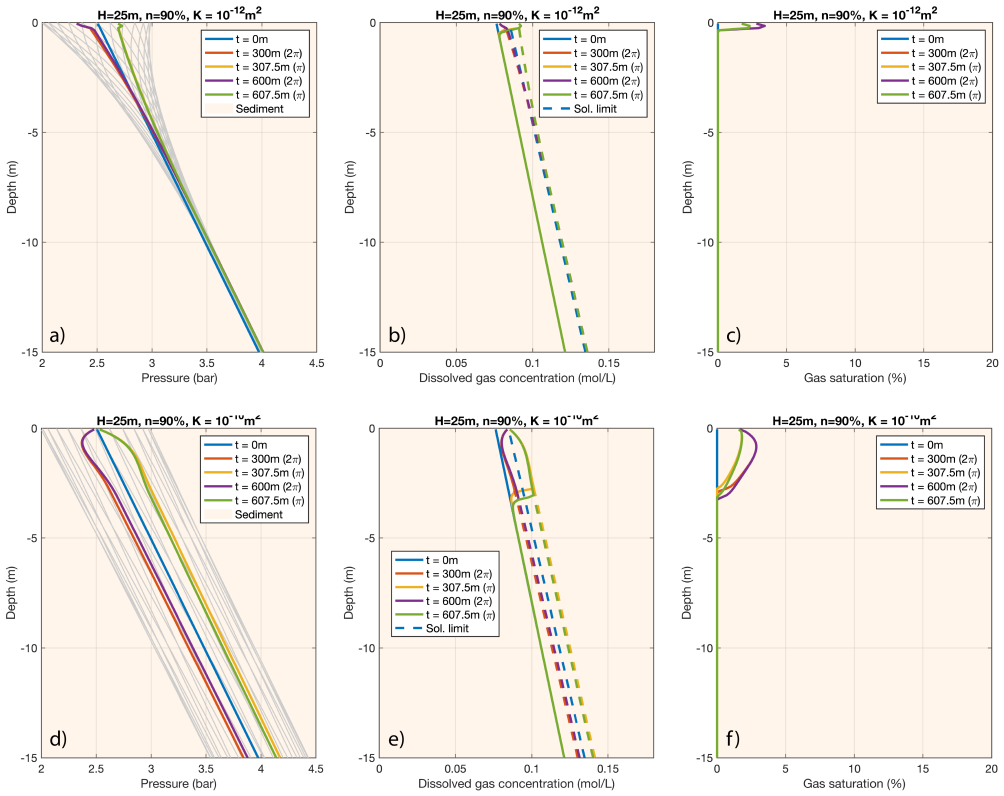

Figure 5: Gas pressure (P_g), saturation (S_g), and dissolved gas concentration (χ_g) for selected scenarios without any pre-existing FGP.

surface (e.g., Fig.5c,f). In turn, due to high compressibility of the resulting free gas, the pressure solution also differs compared to that of the reference sediments. The pressure response is damped over time as more and more free gas appears. The saturation and depth of the free gas layer depend strongly on the sediment permeability. It is important to note that gas compressibility plays an important role in the 'persistence' of the spontaneously formed free gas. If we were to ignore the compressibility effects, the free gas would alternatingly appear and disappear throughout the storm, and a stable free gas phase would not persist. The compressibility of the free gas makes the process irreversible by progressively damping the pressure response during each storm cycle, with the net effect that for each wave more gas appears than that disappears.

In our simulations, we get a gas layer of about 3m for $K = 10^{-10}m^2$ (Fig.5f) but only about a few centimeters for $K = 10^{-12}m^2$ (Fig.5c). For scenarios with $K = 10^{-14}m^2$, no free gas is formed. Absolute water depth also has an influence: for higher H, the gas phase appears with a delay. The controlling mechanism is how the pressure sensitivity of the gas solubility curve varies with hydrostatic pressure. Ultimately, there is a minimum n for any given combination of H and K for which a persisting free gas phase can form near the sea floor. For our control parameters, the minimum n values are listed in Table 1.

Impact of lateral gradients on spontaneous appearance of free gas

The above 1D results show that free gas can spontaneously appear, and even persist, in the upper sediment layers due to the storm induced pressure changes, without

	$K = 10^{-10} m^2$	$K = 10^{-12} m^2$	$K = 10^{-14} m^2$
$H = 25$m	61%	62%	67%
$H = 40$m	76%	76%	79%
$H = 60$m	84%	84%	86%

Table 1: Minimum value of dissolved methane fraction n (upto nearest whole number) for which free gas phase appears in our 2D scenarios.

any pre-existing burried free gas pockets. However, the 1D setting gives a somewhat incomplete picture because a storm is not a standing wave, but rather a travelling wave. A storm forcing creates strong lateral gradients in the sediment which cannot be neglected. In 1D, pressure oscillates around the hydrostatic value, and gas exsolves and dissolves following these pressure changes. In 2D, there is additional transport of the dissolved and the free gas along the lateral pressure gradients. Therefore, it is possible that in some scenarios free gas phase appears and disappears locally with very little or no lateral advection, leading to patchy pools of non-persistent free gas with low S_g, while in other scenarios the lateral advection is large enough to allow the appearance and growth of a persisting gas layer spanning across the full length of the domain (along the sea floor).

We, therefore, also test our hypothesis for a 2D setting where we impose a sinusoidal storm forcing with an amplitude $A = 10$m, time period $T = 12$ seconds and wave length $\lambda = 150$m. Similar to the 1D setting, we assume that the sediment is homogeneous and isotropic, and the domain contains no buried free gas pockets and capillary barriers. Again, we chose the following control parameters: $H\,[m] = \{25, 40, 60\}$, $K\left[m^2\right] = \left\{10^{-10}, 10^{-12}, 10^{-14}\right\}$, and $n\,[\%] = \{70, 80, 90\}$. In total, 27 scenarios were simulated. For numerical simulation, we chose a computational domain with a depth of $z_{domain} =$ 8m and length of $X_{domain} = \lambda$, and the left and right boundaries of the domain are assumed periodic. The upper half of the sediment was discretized with a uniform orthogonal mesh with quadrilateral cells of size $1m \times 0.1m$. The lower half was discretized with an aspect ratio of 1.1 along the depth. Time step size of 2 seconds was used for each scenario, and the total storm duration was set as 10 hours.

The free gas phase appears in local pools and continues to spread laterally to form a continuous free gas phase which eventually spans the entire length of the domain. Similar to the 1D setting, as the storm progresses, the pressure response damps along the sediment depth due to gas compressibility. Furthermore, due to the lateral transport of free gas, the pressure response also shows progressive damping laterally, along the tailing end of each travelling storm-wave. This leads to an asymmetric distribution of free gas phase, with patchy pockets of possibly unstable free gas very close to the seafloor. In Fig.6, a rather prominent free gas layer (with maximum gas saturation of over 6% and depth of nearly 2m) forms over time due to high transport fluxes (both lateral and vertical) owing to high sediment permeability ($K = 10^{-10}$). In contrast, in the equivalent 1D setting, even with high $n = 90\%$, the maximum S_g was only about 3% and the depth was about 3m. appearance of a persisting gas phase strongly depends on the sediment permeability (which controls the transport fluxes). For moderate permeability ($K = 10^{-12}$), a very thin persisting gas layer forms, but for low permeability ($K = 10^{-14}$) small amount of free gas appears and disappears locally, but no persisting gas layer forms (not shown). It is also worth noting that for the scenarios with $H = 40$m, absolutely no free gas phase appears at any time for $n = 70\%$; and for the scenarios with $H = 60$m, no free gas phase appears for $n = 70\%$ and $n = 80\%$. This is consistent with the minimum n values listed in Table 1.

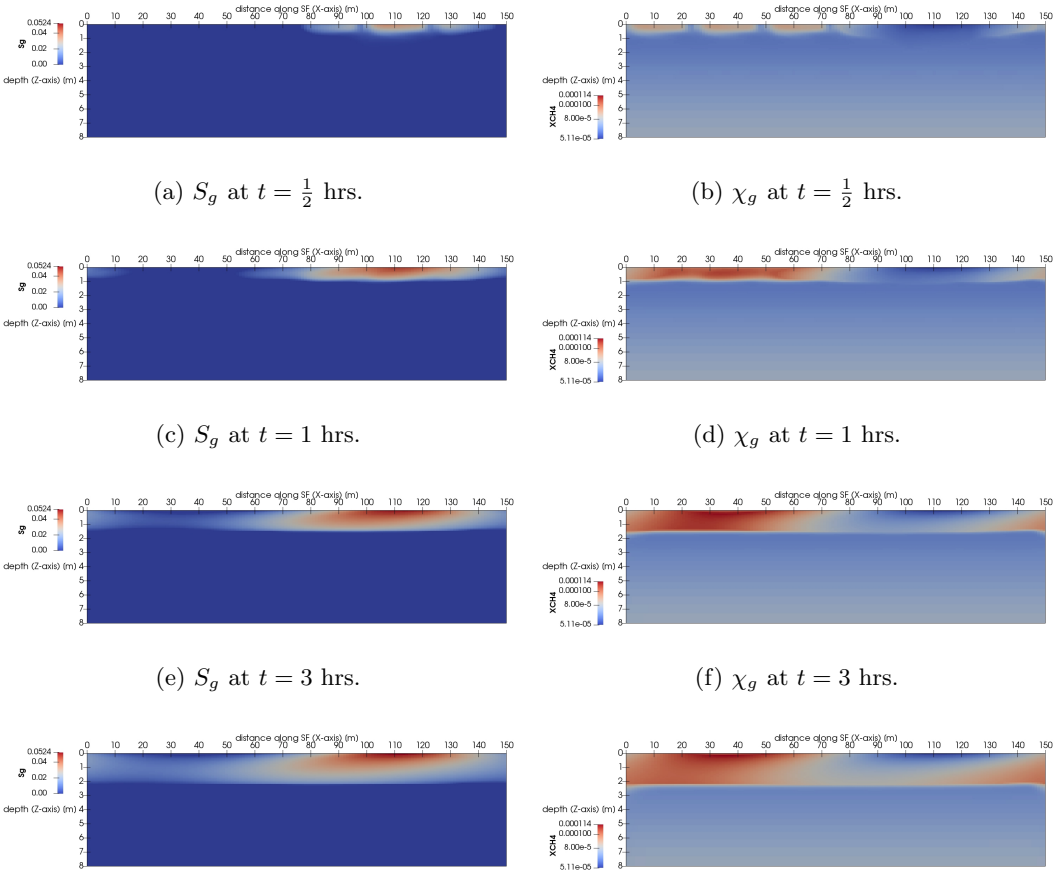

(a) S_g at $t = \frac{1}{2}$ hrs.

(b) χ_g at $t = \frac{1}{2}$ hrs.

(c) S_g at $t = 1$ hrs.

(d) χ_g at $t = 1$ hrs.

(e) S_g at $t = 3$ hrs.

(f) χ_g at $t = 3$ hrs.

(g) S_g at $t = 10$ hrs.

(h) χ_g at $t = 10$ hrs.

Figure 6: Appearance and evolution of a storm induced 'persisting' free gas phase. Figure shows gas saturation S_g and dissolved methane concentration χ_g at different time instants for the case with $H = 25$m, $n = 70\%$, and $K = 10^{-10}m^2$.

Discussion

Understanding pockmark formation involves at least two aspects: The gas source, and the surface manifestation (i.e. mechanical crater) with its feeding system connecting the gas source with shallower strata (e.g. pipe-like conduit at depth). We analyzed, under idealized conditions, the question of the plausible gas sources. Our modelling results show that, even for a barely stable pre-existing FGP (i.e., FGP sealed by a weak capillary barrier) available at some accessible shallow depth, the mobilization of free gas through a simple pumping mechanism is not feasible, as the gas damps the transmission of the storm induced pressure changes. This is consistent and re-confirms findings of previous poro-elastic studies of the pressure response in marine sediments to periodic loading(Wang & Davis, 1996; Van Der Kamp & Gale, 1983; Okusa, 1985). These studies had shown, mainly for tidal forcing, that a layer with reduced fluid/gas bulk modulus will damp any seafloor pressure variations and reduce the penetration depth. Here, building on those studies, we show that one consequence of this damping is that free gas cannot realistically overcome the capillary barrier through rapidly alternating advective fluxes alone. Even if the free gas overcomes the capillary barrier due to gas phase instabilities, it tends to find a quasi-stationary state instead of ascending all the way to the sea floor. In addition we would like to stress that trapping shallow gas at just a few meters below the seafloor is problematic, and not observed in the study area (Karstens et al., 2018; Krämer et al., 2017). The poro-elastic effective stress at such shallow depth is close to the brittle yield stress, so that already small amounts of overpressure, resulting from trapped buoyant gas, might result in seal failure.

Our findings rather point to a different mechanism. For sufficiently high dissolved gas concentrations, depending on the pressure sensitivity of gas solubility, free gas can spontaneously form in the vicinity of the seafloor due to the pressure sensitive phase instabilities. Such a free gas phase may or may not be persistent, and can exist stably only during the storm. This phenomena is likely largely confined to the upper sediment layers. The source of the observed free gas is, therefore, primarily the dissolved gas, which spontaneously changes its phase due to the storm induced pressure perturbations. This gas source is independent of any pre-existing FGPs, and appears to provide a simpler, yet robust, explanation for free gas in storm induced pockmarks, especially in the absence of evidence for such shallow pre-existing gas. In general, however, both these gas sources are not mutually exclusive, and the underlying physics for both is related to the mechanism of pressure sensitive phase instabilities. It is possible that in some settings, both gas sources may be present simultaneously. In such scenarios, the appearance of the persisting free gas phase will greatly enhance because the pre-existing FGP will act as an additional gas reservoir.

For the Helgoland case study, the proposed mechanism appears to be particularly relevant, as none of the existing sub-bottom profiler transects across the area showed any gas pockets in shallow sediments (Krämer et al., 2017; Karstens et al., 2018). However, our results show that it requires a minimum gas saturation of about 60% within the affected pore fluids. The methane gas concentration in the south-eastern North Sea in Pockmark area is about 10 times higher than for background sediments (Krämer et al., 2017), but far below full saturation (Kossel et al., 2013). Hence, a formation of pockmarks by pure methane seems unlikely in the south-eastern North Sea. However, it is plausible that a combination of other dissolved gases together act as a possible gas source. These dissolved gases could be CO_2, O_2 or N_2, some of which show even a greater sensitivity of solubility to pressure changes (Kossel et al., 2013). Saturations of these gases can be, in general, much closer to full saturation, but penetration depths of dissolved O_2 or N_2 are only at cm scale (Neubacher et al., 2013). Furthermore, dissolved gas concentrations can vary significantly on the Helgoland Reef due to different sediment compositions. The Helgoland Reef is traversed by the organic-rich paleo-river deltas of Elbe and Eider, their side arms, and multiple glacial tunnel valleys (Figge, 1980; Lutz et al., 2009; Lohrberg,

Schwarzer, et al., 2020). It is likely that dissolved gas concentrations are higher in the paleo-river beds due to a higher organic matter decomposition (Zhang et al., 2019). Furthermore, differences of the dissolved gas concentrations could explain the spatial distribution of pockmarks in the region. Moreover, the permeability of the south-eastern North Sea is, in general, high, based on sediment composition of mainly fine to medium grain sand (Neumann et al., 2017). Based on numerical models (Neumann et al., 2017), the surface permeabilities can also exhibit local variability due to different sedimentation regimes of the background sediments and the paleo-river deltas of Elbe and Eider. The area where pockmarks occurred in 2015 is characterized by a heterogeneous distribution of permeability. In principle, the permeabilities here can be high, up to ($K = 10^{-10}$) (Neumann et al., 2017). In summary, the proposed mechanism could work on the Helgoland reef, but the gas source(s) and the permeability distribution, and their effects on pockmark formation remain speculative as the necessary data to parameterize and validate the model is missing for this region.

The question about the physical pockmark structures, however, still remains open. These structures likely form due to complex elasto-(plasto-)dynamic interactions between the sediment and the high-frequency storm waves, a study of which lies beyond the scope of this manuscript. Nonetheless, irrespective of the exact mechanisms leading to the formation of these physical structures, we can demonstrate within the scope of our model their potential impact on the subsurface transport processes and the phase instabilities. The high frequency pressure changes potentially alter the porosity-permeability characteristics of the sediment through mechanical feedbacks, which are, for instance, known to form pipe-like fluid pathways in 3-D simulations of compaction-driven fluid flow (Räss et al., 2018). It is likely that the gas build up and the rapidly oscillating pore pressures increase the permeability in the upper sediment layers and aid the appearance of free gas. Furthermore, due to the lateral pressure gradients, it is also likely that the evolution of the permeability field shows a periodic heterogeneity along the sea floor. An example simulation for the scenario with a moderate permeability $K_0 = 10^{-12}m^2$ (Fig.7) illustrates how a simple evolution of permeability field can enhance the free gas layer and periodic high permeability structures can emerge along the sea floor. These high permeability features localize around the peaks of the storm forcing and reflect the inherent time scale of the surface-waves $\leftrightarrow$ bottom-water $\leftrightarrow$ pore-water interactions. This example clearly does not resolve the mechanics of the formation of the actual pockmarks, but provides useful insights into the admissible parameter space for the appearance of a persisting gas phase. In particular, this example demonstrates that the mechanical feedbacks could relax the constraints on the permissible permeability fields and enhance the appearance of persisting free gas phase even in sediments with moderate permeabilities, therefore, enhancing the likelihood of this mechanism. Furthermore, there is a distinct possibility that the mechanical feedbacks may be strong enough to introduce preferential flow paths that run deep enough to support a violent gas ascent of the otherwise quasi-stationary free gas mobilized out of a pre-existing FGP. This introduces a subtle, but very important, distinction between the role of mechanical feedbacks on the plausible gas sources. For pre-existing FGP, the formation of appropriate preferential flow-paths is a 'necessary' condition, thereby, contracting the admissible parameter space; while for spontaneous appearance of free gas, the mechanical feedbacks expand the admissible parameter space.

In general, the process of spontaneous appearance of free gas is likely to occur in shallow marine settings such as shelf regions around the globe. About 50% of shelf areas ($<$ 65 meters water depths) are covered by sand or gravel (Hall, 2002) and meet, therefore, the pre-requisite of high permeability sediments. A similar process has been observed offshore Svalbard (Sultan et al., 2020). Here, exsolution/dissolution during pressure changes of tides has been observed. Although the pressure changes are much slower and no pockmarks occurred, the process is likely based on the here-described mechanism.

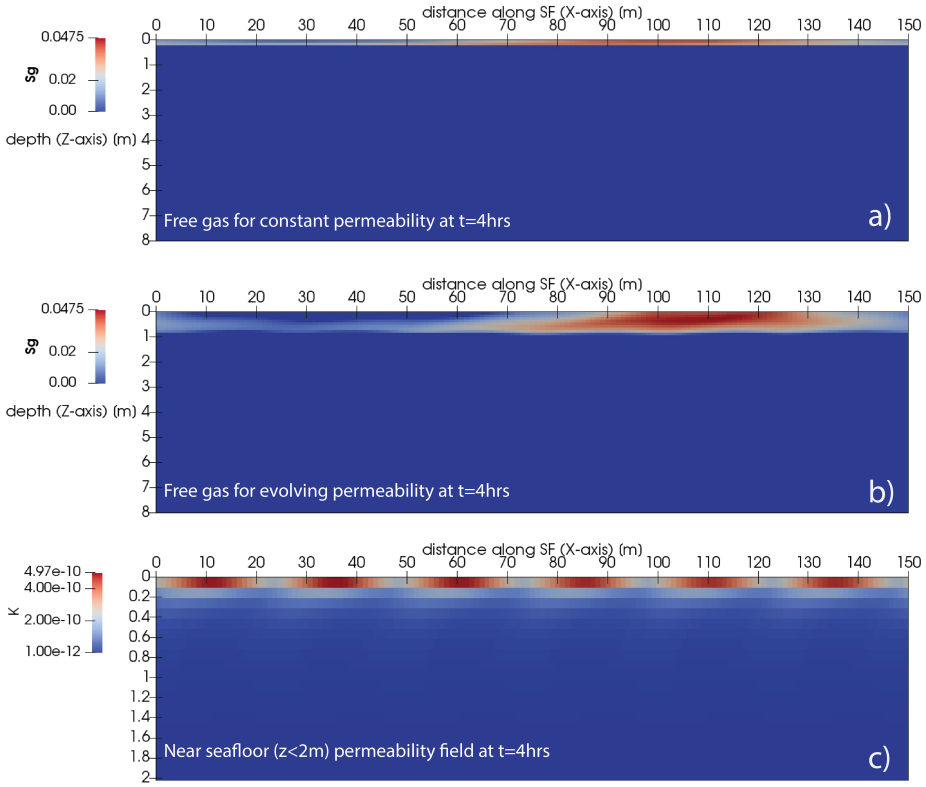

Figure 7: Impact of evolving permeability field due to pressure perturbations. Here, $H = 25$m, $n = 70\%$, and $K = 10^{-12}m^2$. The figure shows following profiles at time $t = 4$ hours: a) Free gas layer with constant permeability field, b) free gas layer with pressure dependent permeability evolution, and c) permeability field (zoomed to upper 2m of the computational domain) where periodic high permeability structures emerge along the sea floor.

The evolution of permeability is modelled using simplified functional relationship between porosity and pressure change as, $d\phi = C\, d\overline{P}$ where, $d\phi$ is change in porosity and $\overline{P} := \sum_{\alpha=g,w} S_\alpha P_\alpha$ is change in effective pore pressure. C is sediment compressibility (assumed constant). In a realistic poro-mechanial setting, C resolves the mechanical coupling conditions and is, therefore, highly non-linear. Permeability is further related to porosity through a power law (Civan, 2001) as, $K = \gamma K_0 \left(\frac{\phi}{1-\phi}\right)^\beta$ where, γ is a proportionality constant, K_0 is permeability of unperturbed sediment, and β is the exponent of the power law. For parameterization, we chose $\phi_0 = 50\%$, $\beta = 6$, $\gamma = \left(\frac{\phi_0}{1-\phi_0}\right)^\beta$, and $C = 1.1e-10$ Pa^{-1} for $d\overline{P} > 0$ and $C = 1.0e-10$ Pa^{-1} for $d\overline{P} < 0$. This relationship is highly simplified and lacks detailed mass and momentum conservation for the sediment phase, but is, nonetheless, a useful qualitative indicator of impacts of pressure changes on the hydraulic properties.

Finally, our findings also suggest that pockmarks may not always be proxies for overpressured shallow gas. Instead, especially in shallow water environments, the ebullition of greenhouse gases from marine sediments in response to long-term variations in seafloor pressure due to e.g. tidal currents or seiches (Lohrberg, Schmale, et al., 2020) and short-term variations due to e.g. high waves (Krämer et al., 2017) may represent additional gas sources. Therefore, global greenhouse gas budgets based on the mere existence of pockmarks without a careful investigation of the source and character of fluids released at the seafloor may lead to misleading results. Furthermore, the spontaneous gas exsolution from pore fluids due to periodic pressure changes at the seafloor could be a potentially significant gas source, which has so far remained unaccounted for in the global gas budgets.

Conclusion

Overall, we offer an explanation for a plausible gas source for storm-induced pockmark formation in shallow marine settings. In contrast to previously suggested processes, our proposed mechanism does not require a pre-existing gas phase or overpressurization of the subsurface. Pressure changes by waves are not only the trigger for fluid/gas migration but also the catalyst for appearance of free gas. Although the released gas volume of a single pockmark may be rather small, the overall worldwide contribution of released greenhouse gases from this mechanism can be significant. The detection of the pockmarks requires a repeated high resolution mapping of target areas and additional careful identification of involved fluids. The absence of these data sets and vanishing of the pockmarks in calm weather conditions can explain why they remain elusive in other areas to date. A corollary of the mechanism described here is that seafloor fluid escape structures are not always proxies for overpressured shallow gas and that spontaneous gas exsolution due to periodic seafloor pressure changes are additional gas sources which may have non-negligible contribution to global gas budgets.

Acknowledgments

SG acknowledges the support of the Cluster of Excellence "The Future Ocean", funded within the framework of the Excellence Initiative by the Deutsche Forschungsgemeinschaft (DFG). The authors further acknowledge the support of AkerBP, Norway.

References

Andreassen, K., Hubbard, A., Winsborrow, M., Patton, H., Vadakkepuliyambatta, S., Plaza-Faverola, A., ... others (2017). Massive blow-out craters formed by hydrate-controlled methane expulsion from the arctic seafloor. *Science*, *356*(6341), 948–953.

Bastian, P., Heimann, F., & Marnach, S. (2010). Generic implementation of finite element methods in the Distributed and Unified Numerics Environment (DUNE). *Kybernetika*, *46*(2), 294–315.

Berndt, C. (2005). Focused fluid flow in passive continental margins. *Philosophical Transactions of the Royal Society A: Mathematical, Physical and Engineering Sciences*, *363*(1837), 2855–2871.

Boetius, A., Ravenschlag, K., Schubert, C. J., Rickert, D., Widdel, F., Gieseke, A., ... Pfannkuche, O. (2000). A marine microbial consortium apparently mediating anaerobic oxidation of methane. *Nature*, *407*(6804), 623–626.

Boles, J., Clark, J., Leifer, I., & Washburn, L. (2001). Temporal variation in natural methane seep rate due to tides, coal oil point area, california [Journal Article]. *Journal of Geophysical Research: Oceans*, *106*(C11), 27077-27086.

Böttner, C., Berndt, C., Reinardy, B. T., Geersen, J., Karstens, J., Bull, J. M., ... Elger, J. (2019). Pockmarks in the witch ground basin, central north sea

[Journal Article]. *Geochemistry, Geophysics, Geosystems*, *20*(4), 1698-1719.

Carter, L. (2010). *Submarine cables and the oceans: connecting the world* (No. 31). UNEP/Earthprint.

Dando, P., Austen, M., Burke Jr, R., Kendall, M., Kennicutt, M., Judd, A., ... Southward, A. (1991). Ecology of a north sea pockmark with an active methane seep. *Marine Ecology Progress Series*, 49–63.

Demmel, J. W., Eisenstat, S. C., Gilbert, J. R., Li, X. S., & Liu, J. W. H. (1999). A supernodal approach to sparse partial pivoting. *SIAM J. Matrix Analysis and Applications*, *20*(3), 720–755.

Dumke, I., Berndt, C., Crutchley, G. J., Krause, S., Liebetrau, V., Gay, A., & Couillard, M. (2014). Seal bypass at the giant gjallar vent (norwegian sea): Indications for a new phase of fluid venting at a 56-ma-old fluid migration system. *Marine Geology*, *351*, 38–52.

Feldens, P., Schmidt, M., Mücke, I., Augustin, N., Al-Farawati, R., Orif, M., & Faber, E. (2016). Expelled subsalt fluids form a pockmark field in the eastern red sea [Journal Article]. *Geo-Marine Letters*, *36*(5), 339-352.

Figge, K. (1980). Das elbe—urstromtal im bereich der deutschen bucht (nordsee) [Journal Article]. *E&G Quaternary Science Journal*, *30*(1), 203-212.

Gupta, S., Wohlmuth, B., & Haeckel, M. (2020). An all-at-once newton strategy for marine methane hydrate reservoir models. *Energies*, *13*(2), 503. doi: 10.3390/en13020503

Hall, S. J. (2002). The continental shelf benthic ecosystem: current status, agents for change and future prospects [Journal Article]. *Environmental Conservation*, 350-374.

Helmig, R. (1997). *Multiphase flow and transport processes in the subsurface. A contribution to the modeling of hydrosystems*. Springer Berlin Heidelberg.

Hoffmann, J., Schneider von Deimling, J., Schröder, J., Schmidt, M., Held, P., Crutchley, G. J., ... Gorman, A. (2020). Complex eyed pockmarks and submarine groundwater discharge revealed by acoustic data and sediment cores in eckernförde bay, sw baltic sea [Journal Article]. *Geochemistry, Geophysics, Geosystems*, *21*(4), e2019GC008825.

Hovland, M., Gardner, J. V., & Judd, A. (2002). The significance of pockmarks to understanding fluid flow processes and geohazards [Journal Article]. *Geofluids*, *2*(2), 127-136.

Hovland, M., & Sommerville, J. H. (1985). Characteristics of two natural gas seepages in the north sea. *Marine and Petroleum Geology*, *2*(4), 319–326.

Judd, A., & Hovland, M. (2007). *Seabed fluid flow: The impact on geology, biology and the marine environment*. Cambridge University Press.

Judd, A., Long, D., & Sankey, M. (1994). Pockmark formation and activity, uk block 15/25, north sea. *Bulletin of the Geological Society of Denmark*, *41*(1), 34–49.

Judd, A. G. (2003). The global importance and context of methane escape from the seabed. *Geo-Marine Letters*, *23*(3), 147–154.

Karstens, J., Schneider von Deimling, J., Böttner, C., Elger, J., Hilbert, H.-S., Kühn, M., ... Schramm, B. (2018). R/v alkor cruise report 512 [al512]-north sea blowouts, 15th july-26th july, 2018, cuxhaven-kiel (germany) [Journal Article]. *RV MARIA S. MERIAN Fahrtbericht/Cruise Report*.

King, L. H., & McLean, B. (1970). Pockmarks on the scotian shelf [Journal Article]. *Geological Society of America Bulletin*, *81*(10), 3141-3148.

Kossel, E., Bigalke, N., Piñero, E., & Haeckel, M. (2013). *The SUGAR Toolbox* [data set]. PANGAEA. doi: 10.1594/PANGAEA.816333

Krämer, K., Holler, P., Herbst, G., Bratek, A., Ahmerkamp, S., Neumann, A., ... Winter, C. (2017). Abrupt emergence of a large pockmark field in the german bight, southeastern north sea [Journal Article]. *Sci Rep*, *7*(1), 5150. doi: 10.1038/s41598-017-05536-1

Leifer, I., & Judd, A. (2015). The uk22/4b blowout 20 years on: Investigations of continuing methane emissions from sub-seabed to the atmosphere in a north sea context. *Marine and Petroleum Geology*, *68*, 706–717.

Lohrberg, A., Schmale, O., Ostrovsky, I., Niemann, H., Held, P., & von Deimling, J. S. (2020). Discovery and quantification of a widespread methane ebullition event in a coastal inlet (baltic sea) using a novel sonar strategy. *Scientific reports*, *10*(1), 1–13.

Lohrberg, A., Schwarzer, K., Unverricht, D., Omlin, A., & Krastel, S. (2020). Architecture of tunnel valleys in the southeastern north sea: new insights from high-resolution seismic imaging. *Journal of Quaternary Science*.

Løseth, H., Wensaas, L., Arntsen, B., Hanken, N.-M., Basire, C., & Graue, K. (2011). 1000 m long gas blow-out pipes. *Marine and Petroleum Geology*, *28*(5), 1047–1060.

Lundsten, E. M., Paull, C. K., Caress, D. W., Gwiazda, R., Cochrane, G. R., Walton, M. A., & Nieminski, N. (2019). Commingled seafloor pockmarks and micro depressions offshore big sur, california [Journal Article]. *AGUFM*, *2019*, EP11B-02.

Lutz, R., Kalka, S., Gaedicke, C., Reinhardt, L., & Winsemann, J. (2009). Pleistocene tunnel valleys in the german north sea: spatial distribution and morphology [pleistozäne rinnen in der deutschen nordsee: Verbreitung und morphologie]. *Zeitschrift der deutschen Gesellschaft für Geowissenschaften*, *160*(3), 225-235.

Neubacher, E. C., Parker, R. E., & Trimmer, M. (2013). The potential effect of sustained hypoxia on nitrogen cycling in sediment from the southern north sea: a mesocosm experiment [Journal Article]. *Biogeochemistry*, *113*(1-3), 69-84.

Neumann, A., Möbius, J., Hass, H. C., Puls, W., & Friedrich, J. (2017). Empirical model to estimate permeability of surface sediments in the german bight (north sea) [Journal Article]. *Journal of Sea Research*, *127*, 36-45.

Okusa, S. (1985). Wave-induced stresses in unsaturated submarine sediments [Journal Article]. *Géotechnique*, *35*(4), 517-532. doi: 10.1680/geot.1985.35.4.517

Plaza-Faverola, A., Bünz, S., & Mienert, J. (2011). Repeated fluid expulsion through sub-seabed chimneys offshore norway in response to glacial cycles [Journal Article]. *Earth and Planetary Science Letters*, *305*(3-4), 297-308.

Räss, L., Simon, N. S. C., & Podladchikov, Y. Y. (2018). Spontaneous formation of fluid escape pipes from subsurface reservoirs [Journal Article]. *Scientific Reports*, *8*(1), 11116. doi: 10.1038/s41598-018-29485-5

Riboulot, V., Thomas, Y., Berné, S., Jouet, G., & Cattaneo, A. (2014). Control of quaternary sea-level changes on gas seeps [Journal Article]. *Geophysical Research Letters*, *41*(14), 4970-4977.

Rollet, N., Logan, G., Kennard, J., O'Brien, P., Jones, A., & Sexton, M. (2006). Characterisation and correlation of active hydrocarbon seepage using geophysical data sets: an example from the tropical, carbonate yampi shelf, northwest australia [Journal Article]. *Marine and Petroleum Geology*, *23*(2), 145-164.

Römer, M., Riedel, M., Scherwath, M., Heesemann, M., & Spence, G. D. (2016). Tidally controlled gas bubble emissions: A comprehensive study using long-term monitoring data from the neptune cabled observatory offshore vancouver island [Journal Article]. *Geochemistry, Geophysics, Geosystems*, *17*(9), 3797-3814.

Sherwood, D., & Dalby, P. (2018). *Modern thermodynamics for chemists and biochemists*. doi: 10.1093/oso/9780198782957.001.0001

Sills, G., & Wheeler, S. (1992). The significance of gas for offshore operations [Journal Article]. *Continental Shelf Research*, *12*(10), 1239-1250.

Sultan, N., Plaza-Faverola, A., Vadakkepuliyambatta, S., Buenz, S., & Knies, J. (2020). Impact of tides and sea-level on deep-sea arctic methane emissions [Journal Article]. *Nature communications*, *11*(1), 1-10.

Talukder, A. R. (2012). Review of submarine cold seep plumbing systems: leakage to seepage and venting. *Terra Nova*, *24*(4), 255–272.

Van Der Kamp, G., & Gale, J. E. (1983). Theory of earth tide and barometric effects in porous formations with compressible grains [Journal Article]. *Water Resources Research*, *19*(2), 538-544. doi: 10.1029/WR019i002p00538

von Deimling, J. S., Linke, P., Schmidt, M., & Rehder, G. (2015). Ongoing methane discharge at well site 22/4b (north sea) and discovery of a spiral vortex bubble plume motion. *Marine and Petroleum Geology*, *68*, 718–730.

von Deimling, J. S., Rehder, G., Greinert, J., McGinnnis, D., Boetius, A., & Linke, P. (2011). Quantification of seep-related methane gas emissions at tommeliten, north sea. *Continental Shelf Research*, *31*(7-8), 867–878.

Wang, K. L., & Davis, E. E. (1996). Theory for the propagation of tidally induced pore pressure variations in layered subseafloor formations [Journal Article]. *Journal of Geophysical Research-Solid Earth*, *101*(B5), 11483-11495. doi: 10.1029/96jb00641

Whiticar, M. J. (2002). Diagenetic relationships of methanogenesis, nutrients, acoustic turbidity, pockmarks and freshwater seepages in eckernforde bay [Journal Article]. *Marine Geology*, *182*, 29-53. doi: 10.1016/S0025-3227(01)00227-4

Yang, D., Li, Q., & Zhang, L. (2015). Propagation of pore pressure diffusion waves in saturated porous media. *Journal of Applied Physics*, *117*(13), 134902. doi: 10.1063/1.4916805

Zhang, W., Wirtz, K., Daewel, U., Wrede, A., Kröncke, I., Kuhn, G., ... Schrum, C. (2019). The budget of macrobenthic reworked organic carbon: A modeling case study of the north sea [Journal Article]. *Journal of Geophysical Research: Biogeosciences*, *124*(6), 1446-1471.

Appendix A Model equations and numerical solution scheme

We consider a homogenized REV (Representative Elementary control-Volume) composed of two distinct mobile phases (also referred as 'fluids'): An aqueous phase (subscript 'w') and a gaseous phase (subscript 'g'). For simplicity, we assume only a single gas in the system (methane in this study), and account for miscibility of the phases. Therefore, the gaseous phase is composed of gas and water vapour, while the aqueous phase is composed of liquid water and dissolved gas. The gas components in both phases are denoted with superscript 'G' and the water components are denoted with the superscript 'H'. For further simplicity, we assume a constant salinity in the aqueous phase and ignore any thermal effects. The component-wise mass conservation for this system can be expressed as,

$$\forall \kappa = G, H: \qquad \sum_{\alpha=g,w} \partial_t \phi \rho_\alpha S_\alpha \chi_\alpha^\kappa + \sum_{\alpha=g,w} \nabla \cdot \rho_\alpha \chi_\alpha^\kappa \mathbf{v}_\alpha + \sum_{\alpha=g,w} \nabla \cdot \phi \rho_\alpha S_\alpha \mathbf{J}_\alpha^\kappa = f^\kappa \quad \text{(A1)}$$

where, ϕ is the porosity, ρ_α is the pressure dependent phase density, S_α is the phase saturation s.t.,

$$\sum_{\alpha=g,w} S_\alpha = 1. \quad \text{(A2)}$$

The variables $\mathbf{v}_\alpha$ denote the phase-wise Darcy velocity fields,

$$\forall \alpha = g, w: \quad \mathbf{v}_\alpha = -\mathbf{K} \frac{k_{r,\alpha}}{\mu_\alpha} \left(\nabla P_\alpha + \rho_\alpha \mathbf{g} \right) \quad \text{(A3)}$$

where, $\mathbf{K}$ is a second order permeability tensor, $k_{r,\alpha}$ is the relative phase permeability, μ_α is the dynamic phase viscosity, and P_α is the phase pore-pressure. We parameterize the capillary pressure across the gas-water phase interface as well as the relative phase permeabilities using the Brooks-Corey model,

$$P_g - P_w := P_c\left(S_w\right) = P_0 S_{w,e}^{-\frac{1}{\lambda}} \quad \text{(A4)}$$

$$k_{r,w} = S_{w,e}^{\frac{2+3\lambda}{\lambda}} \quad \& \quad k_{r,g} = \left(1 - S_{w,e}\right)^2 \left(1 - S_{w,e}^{\frac{2+\lambda}{\lambda}}\right). \quad \text{(A5)}$$

P_0 denotes the gas entry pressure and $\lambda$is a material parameter. $S_{w,e} = \frac{S_w - S_{w,r}}{1 - S_{g,r} - S_{w,r}}$ is the effective water saturation with residual gas and water saturations $S_{g,r}$ and $S_{w,r}$. Note, that the capillary pressure introduces an additional diffusive flux for gas transport ($\nabla P_g = \nabla P_w + \partial_{S_w} P_c \nabla S_w$, where ∇S_w exhibits diffusive characteristics).

A00.1 The variables $\mathbf{J}_\alpha^\kappa$ denote the Fickian diffusion of components κ through any phase α, s.t.,

$$\forall \alpha = g, w \quad \& \quad \forall \kappa = G, H: \quad \mathbf{J}_\alpha^\kappa = -\tau \mathbf{D}_\alpha \nabla \chi_\alpha^\kappa \quad \text{(A6)}$$

where, τ is the tortuosity of the sediment matrix and $\mathbf{D}_\alpha$ is a second order binary diffusion tensor. Additionally, the summation conditions $\sum_{\kappa=G,H} \mathbf{J}_\alpha^\kappa = 0$ hold $\forall \alpha$.

A00.2 The variable f^κ is the volumetric source term for each component $\kappa = G, H$. Within the context of this study, we assume $f^\kappa = 0$.

A00.3 Finally, χ_α^κ are the mole fractions of the components $\kappa = G, H$ in the phase $\alpha = g, w$. If both phases are present, gas and water are assumed to exist in a state of a vapour-liquid equilibrium (VLE), s.t.,

$$\forall \alpha = g, w: \quad \psi_\alpha := 1 - \sum_{\kappa=G,H} \chi_\alpha^\kappa = 0 \quad if \quad S_\alpha > 0. \quad \text{(A7)}$$

The VLE is modelled using the Henry's (eqn.A8) and the Raoult's (eqn.A9) laws,

$$\chi_w^G = H_w^G P_g \chi_g^G \tag{A8}$$

$$\chi_g^H P_g = \chi_w^H P_{sat}^H \tag{A9}$$

where, H_w^G is the pressure dependent solubility coefficient of dissolved gas (i.e. component G in w phase), and P_{sat}^H is the saturation vapour pressure of water vapour (i.e. component H in g phase). From Eqns.A7-A9, it is clear that in a two-phase system, all mole fractions are known a priori as functions of local thermodynamic state (i.e., gas pressure, in this model). These known mole fractions at VLE are commonly referred as 'equilibrium' mole fractions (denoted as $\chi_{\alpha,eq}^{\kappa} \quad \forall \alpha, \kappa$). In other words, in a two-phase system, all mole fractions are dependent variables and the phase saturations are the independently transported quantities.

A00.4 If, however, any of the phases disappear, the VLE condition does not hold, leading to a set of variational inequalities s.t.,

$$\forall \alpha = g, w: \quad \psi_\alpha > 0 \quad if \quad S_\alpha = 0. \tag{A10}$$

Eqn.A10 implies that in a single phase system (e.g. water-only, or gas-only), the solute (i.e., dissolved gas in case of water-only system, and water-vapour in case of gas-only) exists in an under-saturated state, i.e. the solute mole fraction remains below the equilibrium value (also called 'maximum solubility', or simply, 'solubility') corresponding to the local thermodynamic state. The phase saturations degenerate, meaning that the saturation of the vanishing phase is zero while that of the persisting phase is unity. Therefore, in a single phase system, the solute in the persisting phase is transported independently, while the mole fractions of components in the vanishing phase become indeterminate.

A00.5 Eqns.A7 and A10 together form a Kharush-Kuhn-Tucker type constraints,

$$\forall \alpha = g, w: \quad S_\alpha \psi_\alpha = 0. \tag{A11}$$

Eqn.A11 governs the consistent distribution of phase-states and phase transitions from single-phase to two-phase systems and vice versa.

A00.6 Finally, note, that the material properties like phase densities, viscosities, solubility coefficient and saturation vapour pressure, in general, also depend strongly on the temperature, but under the isothermal assumption, this dependence is ignored in this study.

A00.7 The model eqns.A1 and A11 together form a PDAE (partial differential algebraic) system of four governing equations, which is closed by the conditions A2 and A3. We solve for the following primary variables: P_w, S_g, χ_w^G and χ_g^H.

A00.8 The numerical scheme is based on a fully upwinded cell-centered finite volumes method for spatial discretization and an implicit Euler method for temporal discretization. It is capable of solving in 1D, 2D and 3D. The scheme is implemented in DUNE-PDELab (version 2.8) (Bastian et al., 2010) based on C++. For the linearization of the system of governing PDEs, we have implemented a semi-smooth Newton solver which can handle the gas-water phase transitions and appearing and disappearing phases in a mathematically consistent manner. We use a highly optimized SuperLU (Demmel et al., 1999) linear solver for our 1D calculations (which are performed in sequential mode), and a built-in Algebraic Multi-Grid solver for 2D calculations (which are performed in OpenMPI parallel mode). The computations for this study were performed on the high-performance computing cluster at Kiel University (CAU). Further details of our numerical scheme can be found in Gupta et al. (2020)(Gupta et al., 2020).